

# Synthesis and investigations of metal oxides nanoparticles as corrosion inhibitors for copper alloy in sulfuric acid

Haider Nazar Hussein

The General Directorate for Education of Diyala, Diyala, Iraq

## Article Info

### Article history:

Received: 04, 10, 2024

Revised: 10, 04, 2025

Accepted: 03, 05, 2025

Published: 30, 06, 2025

### Keywords:

Metal oxides  
nanoparticles  
polymer  
XRD  
copper alloy  
corrosion

## ABSTRACT

The molecular structure of the zinc oxide, cadmium oxide nanoparticles, and poly [2-N-(allyl) amine-5-(4-chloro phenyl) -1,3,4-thiadiazole] solution was ascertained by FT-IR, HNMR, XRD, TEM, and FE-SEM after the materials were produced. Using a standard microscope and the weight loss method, the corrosion inhibitions of these compounds on copper alloy in 1M sulfuric acid were assessed. The investigation on weight loss demonstrated that these chemicals' inhibitory efficacy varies with solution temperature and rises with increasing weight. Additionally, the different thermodynamic parameters were computed in order to look into the mechanism of corrosion inhibition. The Langmuir adsorption isotherm was followed by the adsorption of nanomaterial the surface of copper alloy in acid. Using a standard microscope, the surface properties of inhibited and uninhibited copper alloy samples were examined. There was more than 85% inhibition. The creation of a protective adsorption surface was due to the significant inhibitory efficiency of the copper alloy. Using standard microscopy, the surface properties of inhibited and uninhibited alloy samples were examined. The calculated values of the thermodynamic functions ( $\Delta G$ ,  $\Delta H$ , and  $\Delta S$ ) on the synthesized samples indicated that the corrosion of the copper alloy is spontaneous, endothermic, and unrandom.

*This is an open access article under the CC BY license.*



## Corresponding Author:

Haider Nazar Hussein

The General Directorate for Education of Diyala  
Baqubah City, Diyala Governorate, Iraq.

Email: [haiderghabee@gmail.com](mailto:haiderghabee@gmail.com)



## 1. INTRODUCTION

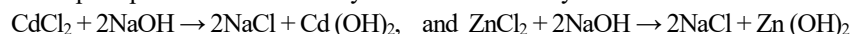
The process of corrosion is a natural occurrence in which an unstable metal in the environment interacts with surrounding elements to become more stable. This interaction results in the formation of oxides or hydroxides, which are then broken down by chemical or electrochemical reactions with the elements in the environment. Iron rust, which is the consequence of iron combining with oxygen or water to generate iron III oxide (rust), and steel rusting and the accompanying deformation with copper, silver, and nickel are examples of metal corrosion [2] [3]. Strength, appearance, fluid permeability, and gas composition are among the attributes and compositions of materials that are diminished by corrosion, it is a significant issue across industries and might seriously affect manufacturing [4]. Vehicle damage is a result of large chemical and electrical power facilities. Pipelines, bridges, guns, and home appliances. However, because corrosion causes significant losses, there is a greater awareness of the need to defend against it these days [5].

Numerous nations have undertaken extensive research to manage corrosion, which is what spurred us to undertake this investigation [6]. Techniques or approaches related to surface morphology are employed in order to analyze and forecast corrosion, image these methods often provide information on surface wear features like pits and fissures. Surface roughness and kind of corrosion [7]. These methods involve microscopes TEM, SEM, and AFM techniques [8] [9] [10]. Because of corrosion, scientists are trying to lessen the financial losses caused by corrosion through research. Several methods and tools have been used as corrective measures. Fortunately, it has been shown that using metal oxide nanoparticles (NPs) can improve corrosion resistance in a variety of severe conditions [11]. As a result, research into the corrosion prevention efficacy of metal oxide nanoparticles with various coating techniques has gained focus. In addition, it is important to clarify and classify the corrosion protection mechanism based on the unique inhibitory properties provided by metal oxide nanoparticles [12]. The key elements influencing the effectiveness of metal oxide nanoparticles' ability to suppress corrosion are well explained in the literature. The issue of corrosion poses a threat to the entire planet and requires significant attention. The use of NPs is justified by their little size, which either slightly wears down metal surfaces or could even increase the metals' resistance to corrosion [13]. Additionally, the barrier qualities of nanocomposites are enhanced by nanoscale metal oxides particles [14]. As a result, NPs are used to create coatings that prevent corrosion [15]. Significant performance was also shown by the functional coatings containing the NPs to strengthen the barrier against corrosive fluids. The creation of functional coatings including NPs is a good fit for the organic coatings [16]. In order to increase corrosion resistance, this chapter calls the reader's attention to the use of metal oxide nanoparticles (NPs) in a 2-N-(allyl) amine-5-(4-chloro phenyl) -1,3,4-thiadiazole as coating.

## 2. Experimental Methodology

### 2.1 Synthesis of CdO and ZnO nanoparticles using the Co-precipitation method.

Cadmium (II) chloride ( $\text{CdCl}_2$ ) and zinc (II) chloride ( $\text{ZnCl}_2$ ) were used in the co-precipitation process to create the CdO and ZnO nanoparticles. Precursor salt (3 g) was dissolved in 100 mL deionized water, and then a 1M NaOH solution was gradually added to the salt solution while being vigorously stirred until the pH reached 12. According to the following equations, sodium hydroxide solution and Cadmium, zinc chloride solution reacted to form a precipitate of Cadmium hydroxide and zinc hydroxide.



After obtaining a precipitate that was yellow and white for  $\text{Cd}(\text{OH})_2$  and  $\text{Zn}(\text{OH})_2$ , respectively, they were repeatedly rinsed with deionized water and 100% ethanol until the pH reached 7. After that, it was dried for an hour at  $70^\circ\text{C}$ . The synthesis pathway is illustrated in Figure 1. Finally, to create cadmium and zinc oxide nanoparticles (CdO and ZnO NPs),  $\text{Cd}(\text{OH})_2$  and  $\text{Zn}(\text{OH})_2$  are calcined for five hours at  $500^\circ\text{C}$  and  $550^\circ\text{C}$ , respectively, in a furnace. According to the following equations:

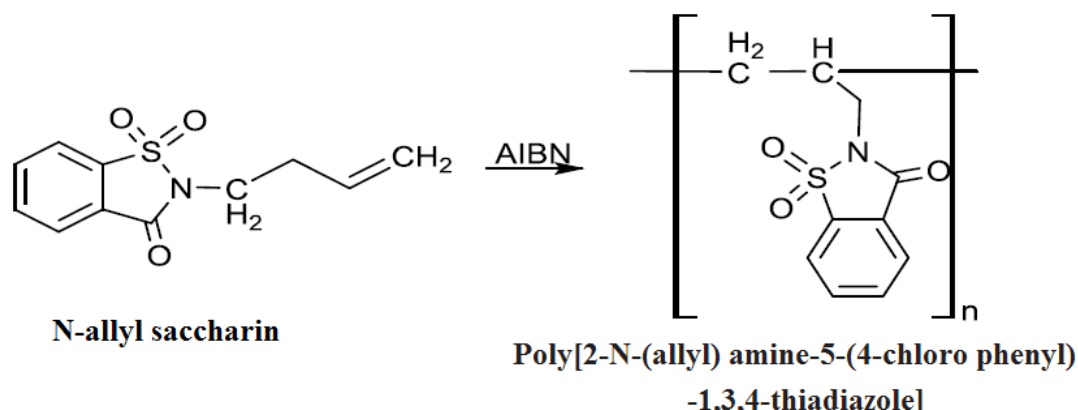
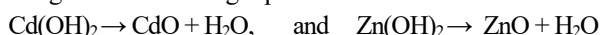


Figure 1: Free-radical polymerization of N-allyl saccharin using AIBN as the initiator to synthesize Poly[2-N-(allyl)amine-5-(4-chlorophenyl)-1,3,4-thiadiazole].

## 2.2 Synthesis of polymer using solution polymerization method.

Solution polymerization was used in the following manner to carry out the polymerization reaction: After dissolving a sodium saccharin compound (0.01 mol) and acrylic acid (0.01 mol, 0.72 g) in 30 milliliters of benzene, the mixture was degassed by nitrogen gas was purged for N – allyl saccharin formed. After cooling, methanol (25 mL) was added, and the mixture was refluxed for 10 hours with AIBN (0.008 mol, 1.3 g) added. This caused the polymer precipitate to develop and solidify on schedule. According to the following equations:

## 3. Corrosion effect study

### 3.1 Samples Preparation and weight loss method

This study examined the corrosion of copper alloys with a 2 mm thickness using a concentration of 1M H<sub>2</sub>SO<sub>4</sub>. The efficiency of ZnO and CdO nanoparticles with poly [2-N-(allyl) amine-5-(4-chlorophenyl)-1,3,4-thiadiazole] suspension in inhibiting corrosion was examined using the weight loss technique. Over the course of 45 days, the test samples were placed in a beaker with varying temperatures (298, 318, 338, and 358 K) in a thermostated water bath. The test samples were submerged in 150 mL of 1M H<sub>2</sub>SO<sub>4</sub> both in the absence and presence of varying weights of ZnO and CdO NPs with poly [2-N-(allyl) amine-5-(4-chlorophenyl)-1,3,4-thiadiazole] as a suspension to corrosion inhibitor. Before being submerged, the samples were weighed first. 45 days later, each piece was removed from the test solution, cleaned with double-distilled water, dried between two filter sheets, and weighed once more using an electronic digital scale. The overall weight reduction was determined by taking the difference in weight. The studies were conducted using 0.2 g of poly [2-N-(allyl) amine-5-(4-chlorophenyl)-1,3,4-thiadiazole] with different weights of nanomaterials as inhibitors (100, 150, 200, 250, 300, 350, 400, 450, and 500 mg). Equations (1), (2), and (3) were used to compute the corrosion rate (CR), the degree of surface covering ( $\theta$ ), and the percentage of inhibitory efficiency (% IE) based on the weight loss findings [17], [18]

$$CR = \frac{\text{weight loss (g)}}{\text{area (m}^2\text{)} \times \text{time (hour)}} \quad (1)$$

where CR is the corrosion inhibition efficiency.

The following formula was used to determine the percentage inhibition efficiency of the weight loss experiments (IE) based on the corrosion rate.

$$IE\% = \frac{CR_{\text{uninhibit}} - CR_{\text{inhibit}}}{CR_{\text{uninhibit}}} \quad (2)$$

where CR<sub>uninhibit</sub> and CR<sub>inhibit</sub>, respectively, represent the corrosion rates in the presence and absence of inhibitors. Degree of Surface Coverage ( $\theta$ )

$$\theta = \frac{W_1 - W_2}{W_1} \quad (3)$$

where  $\theta$  is the inhibitor's degree of surface covering and W<sub>2</sub> and W<sub>1</sub> are the weight losses (mg) for the copper alloy sample in the inhibitor's presence and absence. All analytical grade reagents employed in the experiments are made using deionized water. The weight loss studies were conducted using the following temperature ranges: 298 K, 318 K, 338 K, and 358 K.

## 4. RESULTS AND DISCUSSION

### 4.1 Characterization of polymer using FT-IR spectrum.

Using an FTIR spectrum, the poly [2-N-(allyl) amine-5-(4-chlorophenyl)-1,3,4-thiadiazole] was identified Figure 2. The peaks appeared at 1697, 1597, 1625, 2995–2949, 3074, and 3201, respectively, and indicated the presence of stretching bonds of (C=O), (C=C), (C=N), (C-H aliphatic), (C-H aromatic), and (N-H).

### 4.2 Characterization of polymer using <sup>1</sup>H NMR spectrum.

The polymer's spectrum Figure 3 revealed a double signal for the (CH<sub>2</sub>) group at ( $\delta$ =2.1 ppm), while the proton group (CH-N) produced a trplite signal at (3.7 ppm) and a multiple resonance signal (m) at ( $\delta$ =7.8 ppm) that alluded to the protons in the phenyl ring.

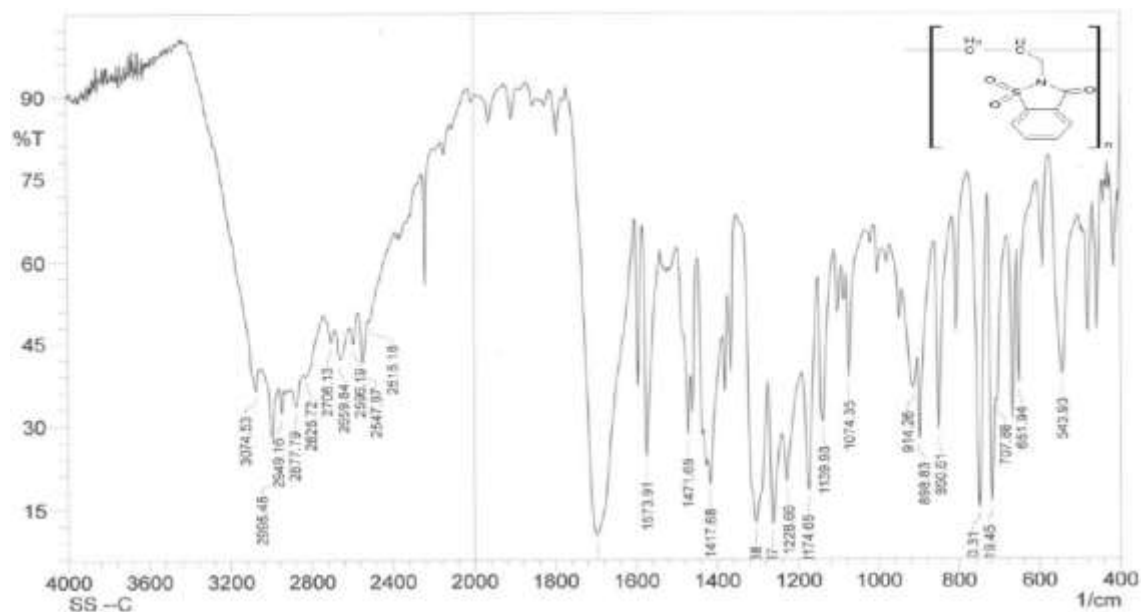


Figure 2: FTIR spectrum for poly [2-N-(allyl) amine-5-(4-chlorophenyl)-1,3,4-thiadiazole]

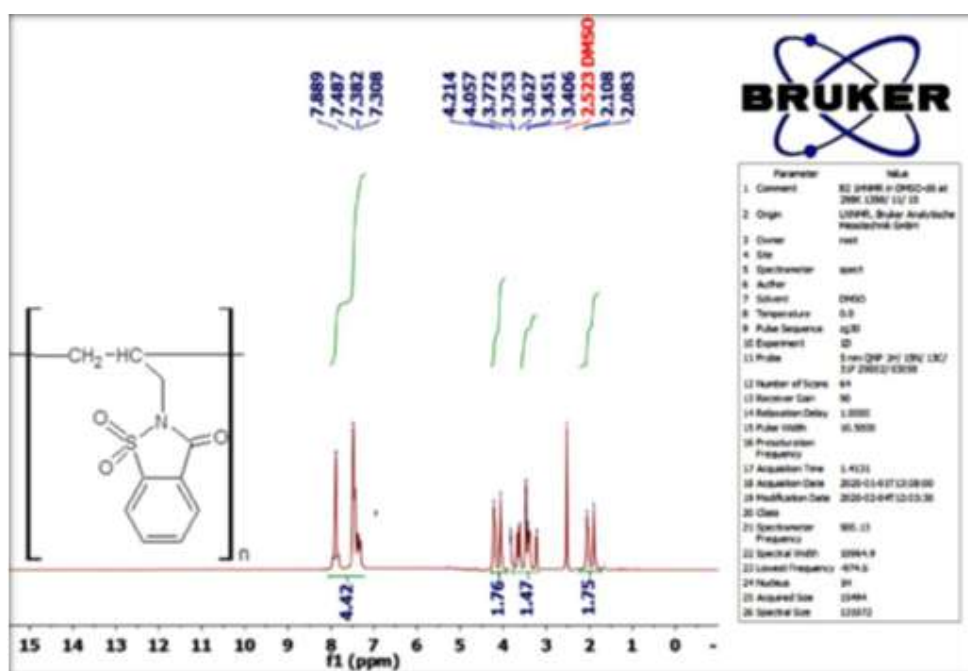


Figure 3: <sup>1</sup>H-NMR spectrum for poly [2-N-(allyl) amine-5-(4-chlorophenyl)-1,3,4-thiadiazole]

#### 4.3 XRD analysis

Figures 4 and 5 display the XRD patterns of the ZnO and CdO nanoparticles that were produced. The prominent peaks indicate that both compounds have a significant degree of crystallinity, which is important to observe. The hexagonal crystal system for ZnO NPs and the cubic structures of CdO NPs are accurately indexed to the majority of the diffraction peaks (JCPDS card nos. 00-101-1003 and 00-901-2914), with corresponding reflection planes of 100, 002, 101, 102, 210, 103, 200, 212, and 201 for ZnO and 111, 200, 220, 311, and 222 for CdO. For the CdO and ZnO NPs generated by co-precipitation, the XRD measurements yielded the lattice constants  $a = 4.6990 \text{ \AA}$  and  $a = 3.2160 \text{ \AA}$  and  $c = 5.2190 \text{ \AA}$ , respectively. The Debye-Scherrer equation indicates that the average size of CdO and ZnO nanoparticles is around 28.92 and 37.09 nm, respectively.

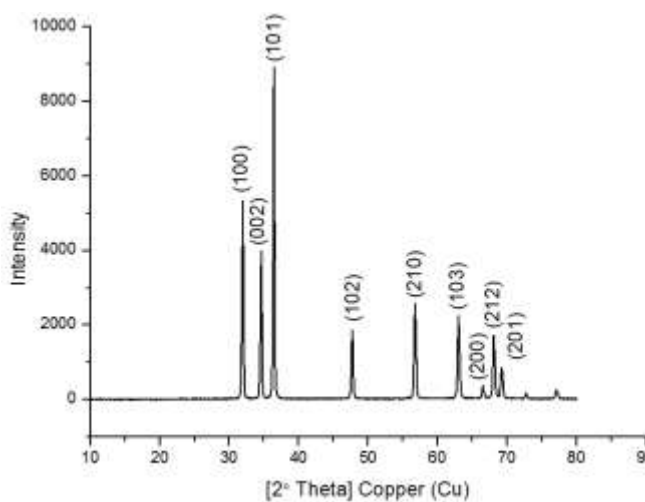


Figure 4: XRD pattern of ZnO NPs prepared by co-precipitation

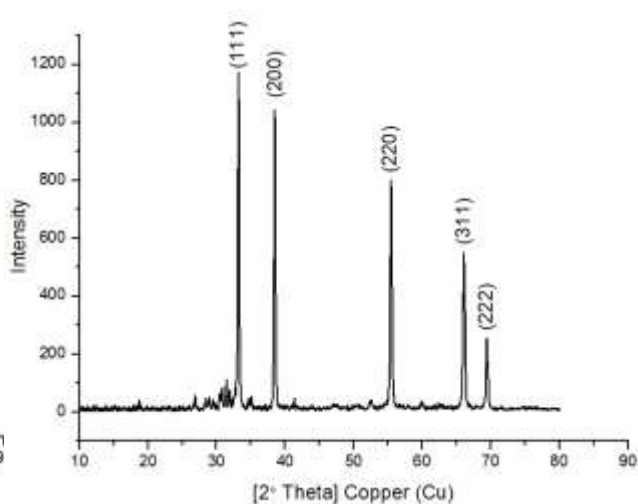


Figure 5: XRD pattern of CdO NPs prepared by co-precipitation.

#### 4.4 FE-SEM images

ZnO and CdO nanoparticles are prepared, and field emission scanning electron microscopy is used to examine the surface morphology of the particles. Figures 6 and 7 show the FE-SEM images of CdO and ZnO nanoparticles. Although the particles have an average diameter of 102 nm, Figure 5 for CdO NPs illustrates how they aggregate to create forms that resemble rods despite their relatively asymmetrical geometries. Figure 6 shows the surface morphology of the ZnO nanoparticle synthesized, which have shapes as islands with average diameter was found to be 195 nm.

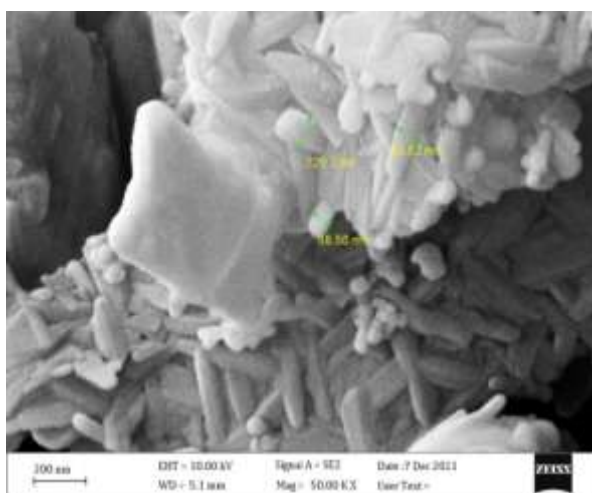


Figure 6: FE-SEM image of CdO NPs synthesized by co-precipitation method.

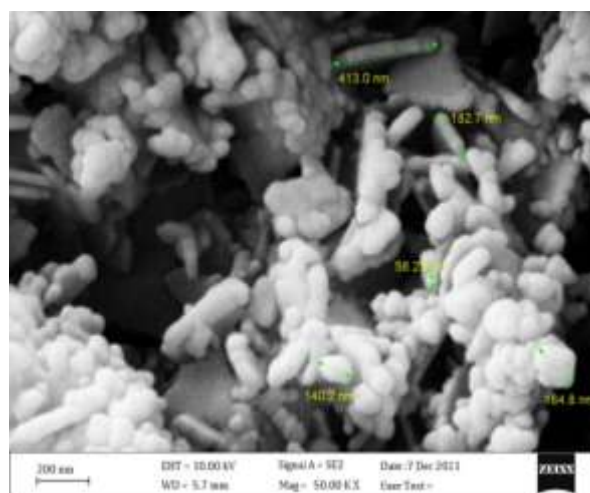


Figure 7: FE-SEM image of ZnO NPs synthesized by co-precipitation method.

#### 4.5 TEM image

Nanoparticles are commonly imaged and analyzed using TEM to ascertain their size, shape, and morphology. TEM images of the CdO and ZnO nanoparticles synthesized by co-precipitation, spherically-shapes are shown in the figures 8 and 9. In addition to the individual nanoparticles, there are also some aggregated ones. The nanoparticle sizes that were identified for CdO nanoparticles ranged from 15 to 42 nm, whereas ZnO nanoparticles produced particle sizes between 36 and 48 nm.

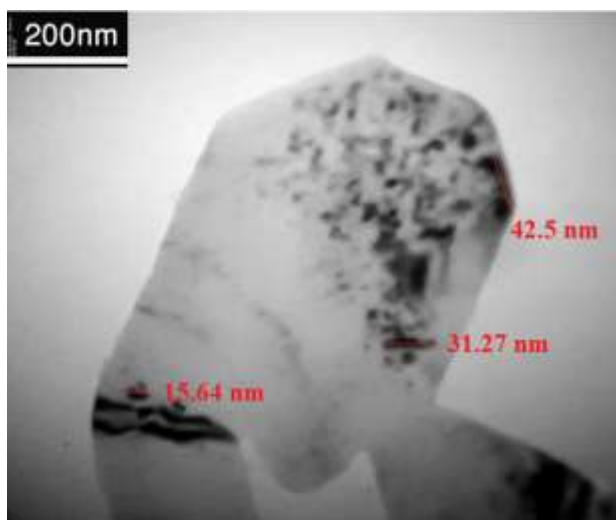


Figure 8:. TEM image of CdO NPs synthezied by co-precipitation method.

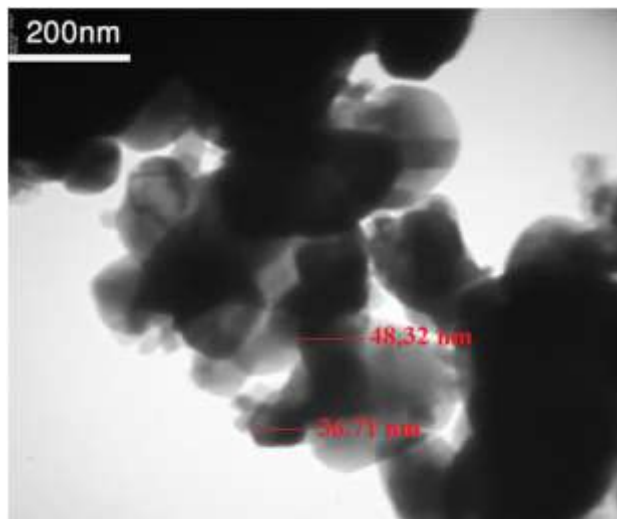


Figure 9: TEM image of ZnO NPs synthezied by co-precipitation method.

### 5. Corrosion results

Zinc oxide and cadmium oxide with poly [2-N-(allyl) amine-5-(4-chlorophenyl)-1,3,4-thiadiazole] as a suspension at all weights under research inhibited the corrosion rate of copper alloy in 1M  $H_2SO_4$ . The inhibition efficacy improves with an increase in inhibitor weight from 100 to 500 mg, as Figures 10 and 11 demonstrate. The maximum degree of inhibitory efficiency was reached at 500 mg, this demonstrates that the nanomaterials experienced desorption can a coating the surface copper alloy and it might be attributed to a variety of other factors, such as the kind and composition of the metal oxide nanoparticles. The effect of temperature on inhibitory effectiveness is seen in Figure 11. The inhibitory effectiveness of all nanomaterial substances decreases as the temperature increases from 298 to 358 K, suggesting that the decrease in inhibitory efficacy with increasing temperature might perhaps be attributed to the desorption of the inhibitor molecules at elevated temperatures.

The degree of surface coverage ( $\theta$ ) for different inhibitor weights in 1M  $H_2SO_4$  at temperature range (from 298 to 358 K) during a 45-day immersion time was estimated based on weight loss measurements. Experimental measurements were made of weight loss ( $\Delta w$ ), corrosion rate (C.R.), percentage of inhibition efficiency (% IE), and degree of surface covering ( $\theta$ ) in 1M  $H_2SO_4$ . Table 1 presents the findings. At varying temperatures, ZnO and CdO nanoparticles with varying weights are combined with poly [2-N-(allyl) amine-5-(4-chlorophenyl)-1,3,4-thiadiazole].

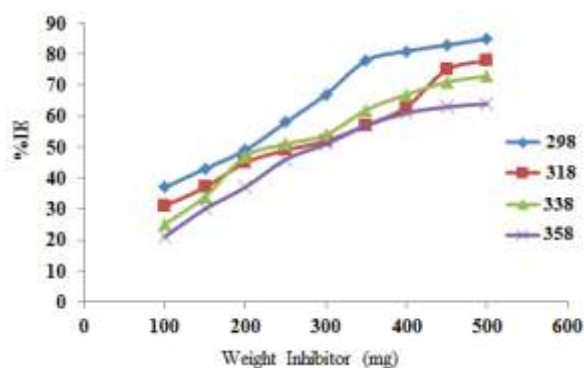


Figure 10: Showing Variation of Inhibition efficiency with ZnO NPs and polymer as an inhibitor weight at different temperatures.

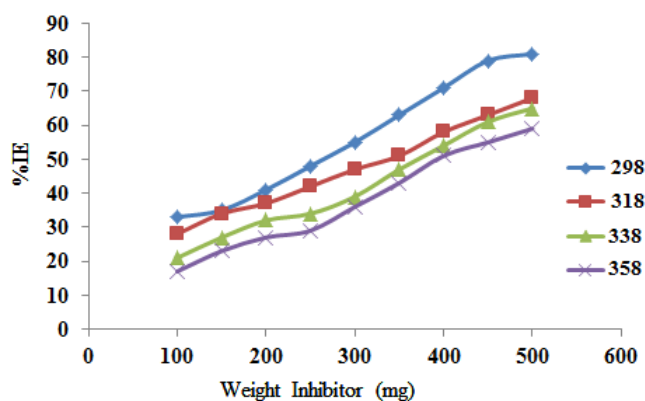


Figure 11: Showing Variation of Inhibition efficiency with CdO NPs and polymer as an inhibitor weight at different temperatures.

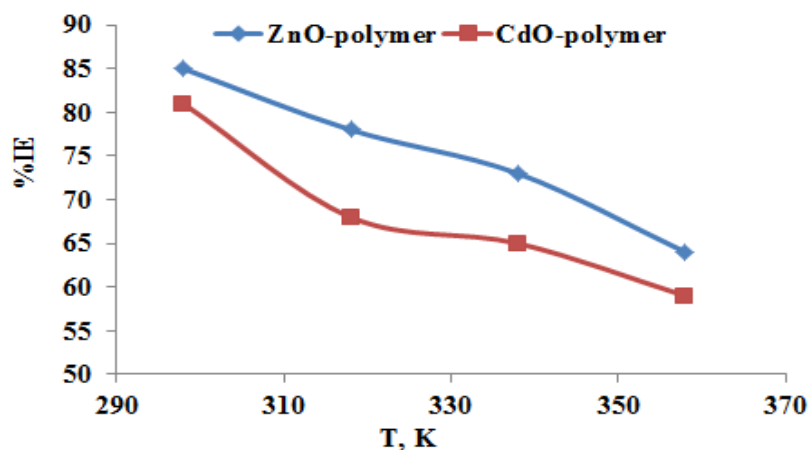


Figure 12: Showing Variation of inhibition efficiency with temperature at a weight of 500 mg by nanomaterials prepared.

Table 1: Weight loss data of copper alloy in 1M H<sub>2</sub>SO<sub>4</sub> (Blank) and in presence of various weight of ZnO NPs, CdO NPs with polymer as a suspension as inhibitors at different temperatures.

Inhibitor	Weight (mg)	Weight Loss in mg ( $\Delta w$ ), Percentage of Inhibition (%I E), Corrosion Rate in mg/cm <sup>2</sup> .d (CR), Surface Coverage ( $\theta$ ) after 45 days, in 1 M H <sub>2</sub> SO <sub>4</sub> .															
		298				318				338				358			
		$\Delta w$ (mg)	% IE	CR	$\theta$	$\Delta w$	% IE	CR	$\theta$	$\Delta w$	% IE	CR	$\theta$	$\Delta w$	% IE	CR	$\theta$
Copper alloy	Blank	175	-	24.31	-	217	-	34.81	-	421	-	48.91	-	653	-	76.23	-
ZnO NPs with Polymer	100	38.2	37	4.13	0.45	71.2	31	11.24	0.31	131.2	25	17.05	0.24	211.3	21	21.37	0.18
	150	36.7	43	4.01	0.49	68.1	37	9.12	0.37	127.3	34	15.47	0.25	205.1	30	17.74	0.21
	200	31.6	49	3.82	0.52	60.2	45	9.05	0.38	115.4	47	14.24	0.29	200.4	37	15.88	0.25
	250	24.9	58	3.61	0.58	58.4	49	8.47	0.41	105.8	51	13.78	0.32	191.3	46	12.09	0.33
	300	19.4	67	3.36	0.63	51.7	52	8.1	0.45	98.3	54	12.81	0.38	184.1	51	11.21	0.36
	350	15.8	78	3.31	0.68	46.3	57	7.12	0.49	93.1	62	11.04	0.45	179.4	57	10.16	0.41
	400	11.1	81	3.03	0.74	42.7	63	6.78	0.52	84.7	67	9.14	0.51	177.3	61	8.92	0.44
	450	10.3	83	2.78	0.75	38.2	75	6.01	0.54	72.8	71	8.56	0.53	173.5	63	8.54	0.47
	500	10.1	85	2.37	0.78	35.6	78	4.23	0.63	66.2	73	7.71	0.54	171.2	64	8.02	0.49
CdO NPs with polymer	100	35.1	33	4.01	0.39	65.4	28	9.91	0.32	124.6	21	14.68	0.21	197.5	17	15.41	0.17
	150	34.3	35	3.88	0.41	63.2	34	9.32	0.34	117.5	27	14.38	0.27	190.8	23	12.18	0.23
	200	30.9	41	3.71	0.46	60.1	37	9.03	0.37	110.1	32	14.01	0.28	181.3	27	11.74	0.27
	250	28.1	48	3.64	0.51	55.2	42	8.81	0.40	103.2	34	13.89	0.33	174.2	29	11.18	0.31
	300	22.6	55	3.46	0.58	50.1	47	8.17	0.44	95.5	39	13.03	0.39	167.9	36	10.78	0.35
	350	18.3	63	3.38	0.65	47.2	51	7.59	0.47	91.9	47	12.45	0.43	161.7	43	10.04	0.42
	400	15.6	71	3.31	0.69	45.8	58	7.08	0.53	86.4	54	11.43	0.49	154.2	51	9.33	0.44
	450	12.5	79	2.88	0.72	42.7	63	6.58	0.55	75.1	61	9.75	0.54	150.1	55	8.79	0.46
	500	11.4	81	2.47	0.74	37.9	68	5.06	0.60	69.8	65	8.59	0.57	146.5	59	8.14	0.47

Figure 13 represents the images taken by the normal microscope of copper alloy before and after

emersion in 1M  $\text{H}_2\text{SO}_4$ , with and without the ZnO and CdO nanoparticles of varying weights and 0.2 g of poly [2-N-(allyl) amine-5-(4-chlorophenyl)-1,3,4-thiadiazole] as suspension inhebaters.

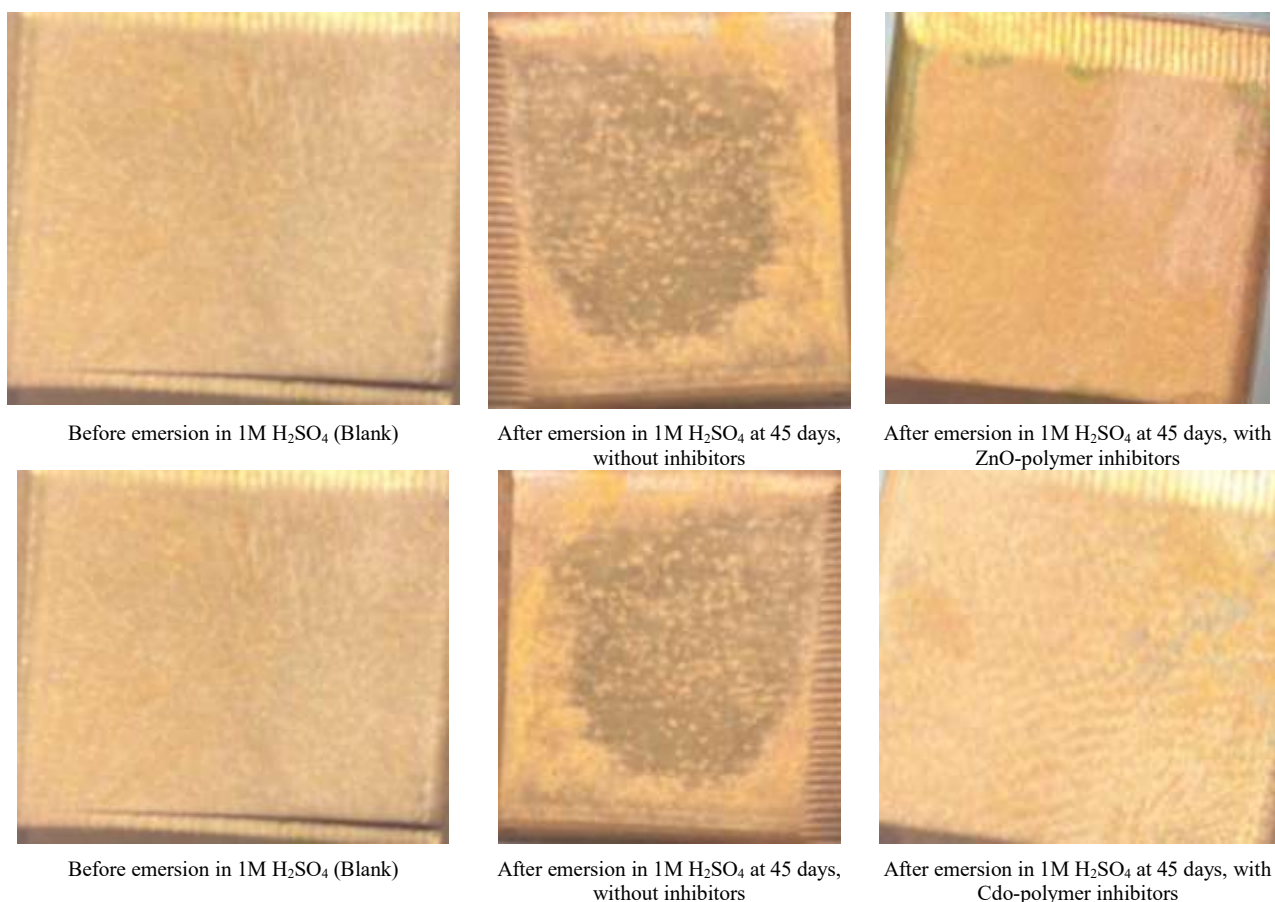


Figure 13: Normal micrographs of Polished copper alloy, After immersion in 1M  $\text{H}_2\text{SO}_4$  for 45 days without corrosion inhibitors, After immersion in 1M  $\text{H}_2\text{SO}_4$  for 45 days with corrosion inhibitors presence of 500 mg.

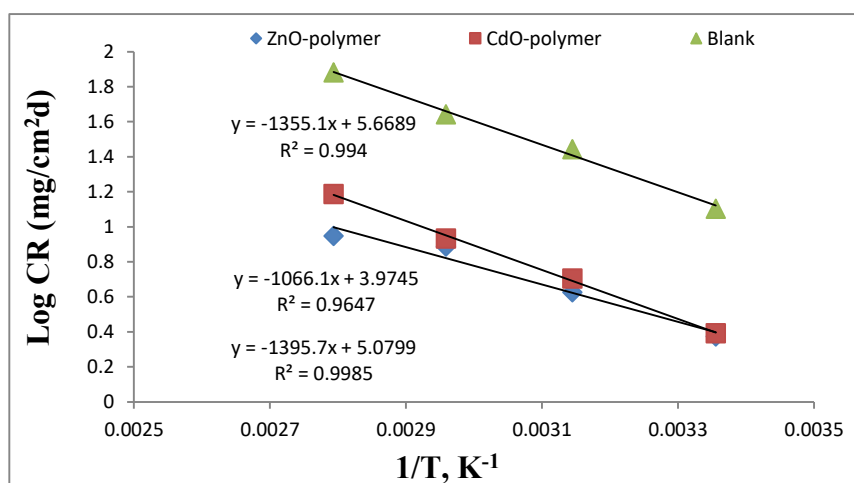


Figure 14: Plots of log (CR) vs.  $1/T$  in Presence of ZnO NPs and CdO NPs with polymer suspension at a weight of 500 mg for copper alloy compare with blank.

### Thermodynamic activation parameters

The plot of  $\log(CR)$  against  $1/T$  is shown in Figure 14. The slope ( $E_a/2.303R$ ) of the curve is used to calculate the activation energy ( $E_a$ ), and the findings are displayed in Table 2. ZnO-polymer, CdO-polymer, and Blank have activation energy ( $E_a$ ) values of 8305.9 J mol<sup>-1</sup>, 8496.901.1 J mol<sup>-1</sup>, and 7222.985 J mol<sup>-1</sup>, respectively. The Arrhenius equation states that the logarithm of the corrosion rate in an acidic solution is a linear function of  $1/T$ , as per the writings of Breslin CB (1993), Rehim SSA (2001), and Khedr M. G. (1992).

$$\log(CR) = \log A - \frac{E_a}{2.303 RT} \quad (4)$$

where A is the Arrhenius pre exponential factor, R is the universal gas constant (8.314 J.mol<sup>-1</sup> K<sup>-1</sup>), and  $E_a$  is the activation energy. According to results, the activation energy ( $E_a$ ) values for the inhibited system are higher than those for the uninhibited system (Blank), indicating that the dissolution of copper alloy is sluggish when inhibitors are present. Equation (5) indicates that a greater  $E_a$  value corresponds to a lower rate of corrosion. This is because a coating that acts as a barrier of protection has formed on the surface of the copper alloy. For copper alloys, the inhibitory efficiency is ZnO-polymer > CdO-polymer. It can be seen from the thermodynamic parameter values that the inhibitors work best at lower temperatures. The transition state equation is an alternate formula for the Arrhenius equation (5) [19]:

$$\log \frac{CR}{T} = \log \frac{R}{Nh} + \frac{\Delta S}{2.303R} - \frac{\Delta H}{2.303RT} \quad (5)$$

where N is the Avogadro number, h is the Plank constant,  $\Delta S$  is the entropy of activation, and  $\Delta H$  is the enthalpy of activation. Plotting  $\log(CR/T)$  versus  $1/T$  yielded a straight line with a slope of  $(-\Delta H/2.303 R)$  and an intercept of  $[(\log(R/Nh) + (\Delta S/2.303 R))]$  (Figure 15). The values of  $\Delta S$  and  $\Delta H$  were calculated from this line. as seen in Table 2.

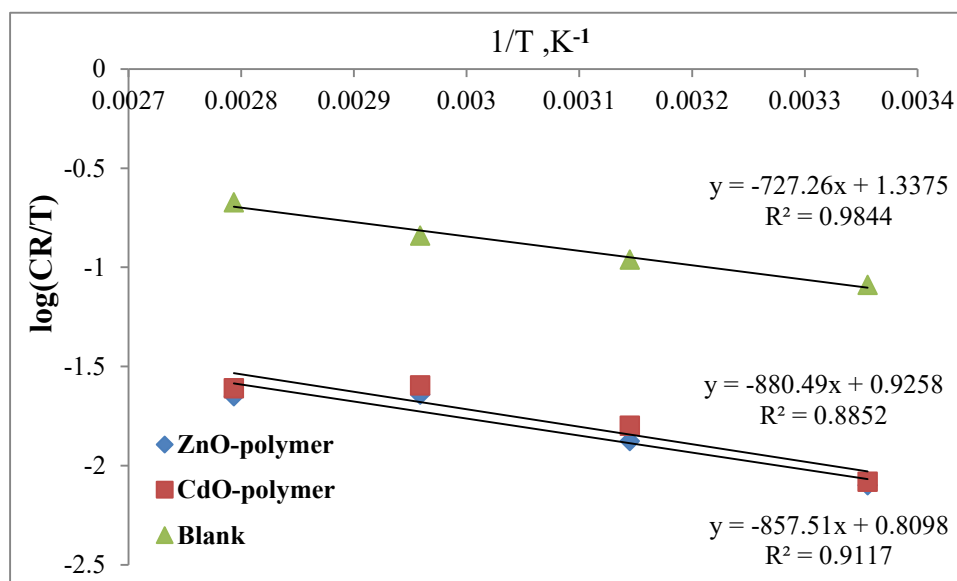


Figure 15: Plots of  $\log(CR/T)$  vs.  $1/T$  in Presence of ZnO-polymer and CdO - polymer as a suspension at a weight of 500 mg at 45 days immersion time for copper alloy

For copper alloy, the enthalpy of activation values ( $\Delta H$ ) are in the following order: CdO-polymer > ZnO-polymer > blank. The corrosion process is endothermic, as indicated by the positive values of  $\Delta H$ . Because  $\Delta S$  is negative in both inhibitor-containing and inhibitor-free scenarios, it is possible that the complex's activation during the rate-determining step represents an association rather than a dissociation step. This indicates that as the state changes from reactants to the activated complex, disordering increases. The findings displayed in Table 2 demonstrate that  $\Delta S^*$  decreased (to larger negative values) in the presence of the inhibitor under investigation as contrasted to a blank (free H<sub>2</sub>SO<sub>4</sub> solution).

Because the transition state of the rate-determining recombination phase suggests a more ordered arrangement compared to the initial state in the inhibitory presence, a high value for the entropy of activation is created. But when nanomaterial compounds are adsorbed onto copper alloy surfaces when an inhibitor is present, that's when the rate-determining phase happens. The inhibitor molecules covering the surface will cause the corrosion at the copper alloy surface to be delayed, which will increase the entropy of activation and cause an unrandomness arrangement in the system. An increase in  $\Delta S^*$  (-171.966 to -182.06 J/mol) upon the addition of an inhibitor suggests increased disordering during the transition from reactant to activated complex. This phenomena may be explained by the process of nanomaterial molecules adhering to the copper alloy surface.

Table 2. Thermodynamic activation parameters for dissolution of copper alloy in 1M H<sub>2</sub>SO<sub>4</sub> and in presence of 500 mg of ZnO-polymer and CdO-polymer inhibitor.

Sample	Ea (kJ mole <sup>-1</sup> )	$\Delta H^*$ (kJ mole <sup>-1</sup> )	$\Delta S^*$ (J mole <sup>-1</sup> K <sup>-1</sup> )
Blank	7.223	13.924	- 171.966
ZnO-polymer	8.306	16.418	- 182.06
CdO- polymer	8.497	16.858	- 179.84

### Adsorption Isotherms

The adsorption behavior of ZnO-polymer and CdO-polymer inhibitors was found to be best described by the Langmuir adsorption isotherm (figures 16 and 17), which obeys the following equation:

$$\frac{C_{inh}}{\theta} = \frac{1}{K_{ads}} + C_{inh} \quad (6)$$

where the adsorption constant is  $K_{ads}$ , the intercept lines on the  $C_{inh}/\theta$  axis can be used to calculate the  $K_{ads}$  values. Equation 7 connects this to the conventional free energy of adsorption ( $\Delta G^\circ$ ).

$$\Delta G^\circ = -RT \ln(55.5 K_{ads}) \quad (7)$$

where the solution's mL/L water content is 55.5. Table 3 displays the  $\Delta G^\circ$  values for the inhibitor on the copper alloy surface. The spontaneity of the adsorption process and the stability of the adsorbed layer on the copper alloy surface are shown by the negative values of  $\Delta G^\circ$ . As the temperature increased,  $\Delta G^\circ$  declined (became more negative), suggesting the presence of an endothermic activity.

Inorganic and organic inhibitors of metallic corrosion rely on adsorption to some extent. Understanding the mechanism of suppression of the corrosion response of metals and alloys requires an understanding of adsorption isotherms. Generally, atoms of oxygen, nitrogen, and sulfur are involved in the adsorption of organic molecules on a metallic surface. Adsorption occurs in ZnO and CdO polymers suspension because of oxygen atoms in the polymer structure. By blocking active sites on the surface of the copper alloy, this procedure may lessen the metal's corrosiveness. Presuming that the inhibitors deposited on the alloy surface reduce the surface area accessible for corrosion processes, Due to their increased electron density, the oxygen atoms in the polymer function as the reaction centers (polar function), causing a monolayer to develop on the metal surface [20]. Most people agree that a crucial stage in the inhibition process is the inhibitor adsorption on the metal surface [21]. Several isotherms were investigated, and the curve fitting of corrosion data in 1M H<sub>2</sub>SO<sub>4</sub> with varying weights of nanomaterials at 298 K was assessed in order to identify the adsorption mechanism.

Table 3. Calculated free energy  $\Delta G^\circ_{ads}$  values of ZnO-Polymer and CdO-Polymer as a suspension inhibitors for copper alloy in 1 M H<sub>2</sub>SO<sub>4</sub> at different temperatures.

sample	Temperature, K			
	298	318	338	358
ZnO-Polymer	-5.44356	-6.9637	-8.96604	-10.0763
CdO-Polymer	-6.18694	-7.08625	-9.13522	-9.89757

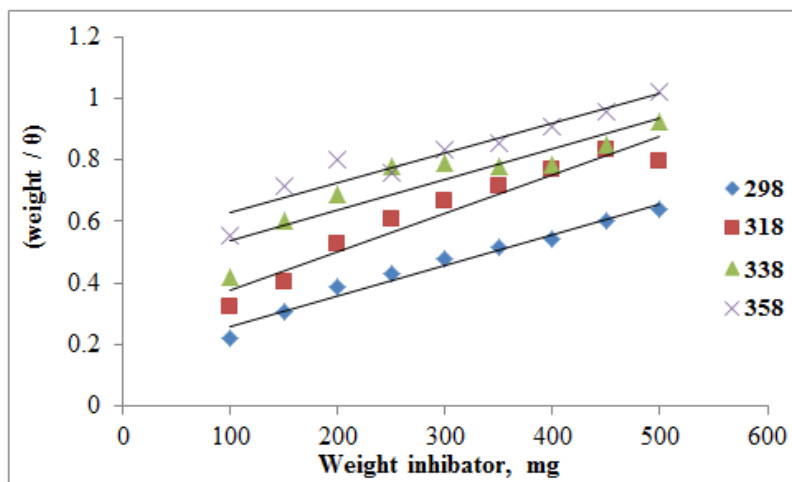


Figure 16: Langmuir adsorption isotherm plots for copper alloy in 1 M H<sub>2</sub>SO<sub>4</sub> with different weight of ZnO-Polymer.

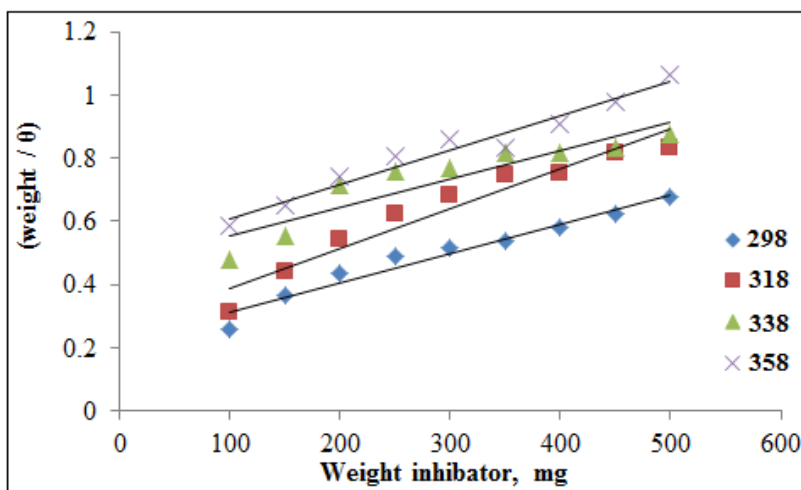


Figure17: Langmuir adsorption isotherm plots for copper alloy in 1 M H<sub>2</sub>SO<sub>4</sub> with different weight of CdO-Polymer

## 6. CONCLUSION

In a 1M sulfuric acid solution, the studied zinc oxide, cadmium oxide nanoparticles, and poly [2-N-(allyl) amine-5-(4-chloro phenyl)-1,3,4-thiadiazole] as a suspension are effective inhibitors for copper alloy. In studies on weight loss, all suspensions of nanomaterials and polymers show an increase in inhibitory efficiency (IE) with an increase in inhibitor weight but a reduction with an increase in immersion temperature. The order of the percentage inhibition (% IE) is as follows: For a copper alloy, ZnO-polymer > CdO-polymer > blank. The Langmuir adsorption isotherm is followed by the suspensions of ZnO and CdO polymers when they adsorb on the alloy surface in a 1M H<sub>2</sub>SO<sub>4</sub> solution. The spontaneous nature of adsorption is indicated by the negative values of  $\Delta G_{ads}$ , indicating that desorption is the mechanism responsible for inhibiting corrosion. Due to the creation of a protective barrier coating, inhibited alloy samples have a smoother surface than uninhibited samples, according to the normal microscopy method.




## ACKNOWLEDGEMENTS

The authors appreciate the College of Education for Pure Sciences - University of Diyala - for using laboratories with the necessary equipment to carry out the experiment.

## REFERENCES

- [1] M. A.-A. Allah, et al., "Application of Machine Learning and Deep Learning Techniques for Corrosion and Cracks Detection in Nuclear Power Plants: A Review," Arabian Journal for Science and Engineering, pp. 1-29, 2024.
- [2] D. S. Dunn, et al., "Corrosion of iron under alternating wet and dry conditions," in NACE CORROSION, 1999, pp. NACE-99223.
- [3] A. Ouarga, et al., "Corrosion of iron and nickel based alloys in sulphuric acid: Challenges and prevention strategies," Journal of Materials Research and Technology, 2023.
- [4] K. Chen, et al., "Study on corrosion resistance and hydrogen permeation behavior in inter-critically reheated coarse-grained heat-affected zone of X80 pipeline steel," Metals, vol. 12, p. 1203, 2022.
- [5] H. L. Lim and E. Gunister, "Awareness of corrosion importance among engineering undergraduates in the United Arab Emirates," Educational Research, vol. 9, pp. 021-034, 2018.
- [6] U. M. Angst, "Challenges and opportunities in corrosion of steel in concrete," Materials and Structures, vol. 51, p. 4, 2018.
- [7] B. Nie, et al., "Surface morphology characteristics and mechanical properties of corroded cold-formed steel channel sections," Journal of Building Engineering, vol. 42, p. 102786, 2021.
- [8] S. Simeonova, et al., "Atomic force microscopy/AFM/study of the surface morphology of TiO<sub>2</sub> featuring with Sm<sub>2</sub>O<sub>3</sub> films obtained by the sol-gel method," Materials Science. Non-Equilibrium Phase Transformations., vol. 6, pp. 71-72, 2020.
- [9] Z. Song and Z.-H. Xie, "A literature review of in situ transmission electron microscopy technique in corrosion studies," Micron, vol. 112, pp. 69-83, 2018.
- [10] G. Fytianos, et al., "Corrosion Evaluation of MEA Solutions by SEM-EDS, ICP-MS and XRD," Energy Procedia, vol. 86, pp. 197-204, 2016.
- [11] M. Ozdincer and S. Durmus, "Fabrication, characterization and corrosion inhibition properties of SCW-based ZnO nanofluids," Chemical Engineering Communications, vol. 211, pp. 476-491, 2024.
- [12] R. Sesia, et al., "Natural polyphenols and the corrosion protection of steel: Recent advances and future perspectives for green and promising strategies," Metals, vol. 13, p. 1070, 2023.
- [13] G. Bahlakeh, et al., "Cerium oxide nanoparticles influences on the binding and corrosion protection characteristics of a melamine-cured polyester resin on mild steel: an experimental, density functional theory and molecular dynamics simulation study," Corrosion Science, vol. 118, pp. 69-83, 2017.
- [14] L. M. Muresan, "Nanocomposite coatings for anti-corrosion properties of metallic substrates," Materials, vol. 16, p. 5092, 2023.
- [15] Z. Z. Ali, et al., "Investigation Nano-coating for the Corrosion Protection of Petroleum storage tanks Steel," Engineering and Technology Journal, vol. 40, pp. 1605-1613, 2022.
- [16] U. Eduok, et al., "Synthesis and characterization of anticorrosion zirconia/acrylic nanocomposite resin coatings for steel," Progress in Organic Coatings, vol. 137, p. 105337, 2019.
- [17] S. K. Ahmed, et al., "Synthesis and investigations of heterocyclic compounds as corrosion inhibitors for mild steel in hydrochloric acid," International Journal of Industrial Chemistry, vol. 10, pp. 159-173, 2019.
- [18] A. Hamdy and N. S. El-Gendy, "Thermodynamic, adsorption and electrochemical studies for corrosion inhibition of carbon steel by henna extract in acid medium," Egyptian Journal of Petroleum, vol. 22, pp. 17-25, 2013.
- [19] L. Herrag, et al., "The effect of 3-cyclohexylamino-propionitrile and aminocyclohexane on the behaviour steel in HCl solution," Der Pharma Chemica Journal, vol. 4, pp. 1522-1534, 2012.
- [20] H. Asfour, et al., "Synthesis and characterization of new polymeric ionic liquids as corrosion inhibitors for carbon steel in a corrosive medium: Experimental, spectral, and theoretical studies," ACS omega, vol. 8, pp. 41077-41099, 2023.
- [21] F. Kaya, et al., "Adsorption and corrosion inhibition capability of Rheum ribes root extract (Işgın) for mild steel protection in acidic medium: A comprehensive electrochemical, surface characterization, synergistic inhibition effect, and stability study," Journal of Molecular Liquids, vol. 372, p. 121219, 2023.

## BIOGRAPHIES OF AUTHORS

	<p>Mr. Haider Nazar Hussein holds a master in physical chemistry and is a lecturer in the general direction for education of Diyala.  Email: <a href="mailto:haiderghabee@gmail.com">haiderghabee@gmail.com</a></p> <div style="display: flex; justify-content: space-around; align-items: center;">   </div>
---	---